Development of a Methodology for Parametric Analysis of STOL Airpark Geo-Density

Joseph N. Robinson*, Max-Daniel Sokollek†, Cedric Y. Justin‡, and Dimitri N. Mavris§
Georgia Institute of Technology, Atlanta, Georgia, 30332-0150, United States

Vehicles designed for urban air mobility (UAM) or on-demand mobility (ODM) applications typically adopt an architecture enabling vertical takeoff and landing (VTOL) capabilities. UAM or ODM systems featuring these capabilities typically have a smaller ground footprint but are subject to a number of performance compromises that make sizing and optimizing the vehicles more challenging. These design challenges can be further compounded when additional environmental considerations are taken into account and in particular if electric propulsion is considered. Alternative architectures such as short takeoff and landing (STOL) and super-short takeoff and landing (SSTOL) vehicles are thus investigated because they present possible advantages in terms of energy efficiency, overall vehicle performance, and noise footprint. However, the larger ground footprint of the infrastructure necessary to operate these systems means that these systems may be more difficult to integrate into a urban and suburban environment. One objective of this research is to estimate the geo-density of airparks suitable for STOL and SSTOL operations based on vehicle performance and ground footprint parameters. In turn, this helps establish requirements for the field performances of STOL and SSTOL vehicles to be considered for ODM and UAM applications. This research proposes and interactive and parametric design and trade-off analysis environment to help decision makers assess the suitability of candidate cities for STOL and SSTOL operations. Preliminary results for the Miami metropolitan area show that an average airpark geo-density of 1.66 airparks per square mile can be achieved with a 300 foot long runway.

I. Introduction

In recent years, a significant amount of effort has gone into developing efficient and environmentally responsible forms of aerial transportation in order to reduce ground-traffic congestion and provide alternative travel options to the public. Two dominant transportation concepts of operation have emerged: on-demand urban air mobility (UAM), which focuses on providing on-demand aerial transportation using small vehicles in dense urban centers, and thin-haul aviation, which seeks to take advantage of the country's underutilized general aviation airports using scheduled services operated by nine-passenger vehicles over short distances. UAM operations, such as those being planned by Uber, are typically focused on distances of approximately 50 nmi [1]. Thin-haul vehicles are planned to operate in the 150 to 300 nmi range [2, 3]. However, there are a number of potentially profitable routes in the 50 to 150 nmi range that can be served by a new class of vehicles specifically designed to serve this suburban air mobility (SUAM) market. This market could neither be served by electric VTOL vehicles for lack of range nor by thin haul vehicles for lack of runway density. Customers of these services could be frequent long-distance commuters willing to travel from their homes in the extended suburbs to the nearest international airport, or executives in the Northeast traveling from their offices in New York or Connecticut to their holiday homes in the Hamptons.

While the dense urban areas served by UAM may require a VTOL aircraft to minimize the footprint of landing zones and comply with overflight requirements, the longer distances covered by thin-haul aviation essentially drive the need for fixed-wing architectures for efficiency reasons. However, for missions between 50 and 150 nmi, the vehicle architecture selection does not seem to be so tightly bounded by efficiency and footprint constraints and thus the design space may be more open. Although a large number of prior studies on UAM [4–6] have focused on VTOL aircraft, UAM and SUAM markets may be better served by STOL or SSTOL vehicles.

*Graduate Research Associate, Aerospace Systems Design Laboratory, AIAA Student Member
†Graduate Research Associate, Aerospace Systems Design Laboratory
‡Research Engineer II, Aerospace Systems Design Laboratory, AIAA Member
§S.P. Langley NIA Distinguished Regents Professor, Boeing Professor of Advanced Aerospace Analysis, Director of the Aerospace Systems Design Laboratory, AIAA Fellow

A. Disadvantages of VTOL Aircraft

Although VTOL aircraft excel at operations where field-length is limited, they possess a number of unavoidable compromises over fixed-wing aircraft. The most critical disadvantage is the necessary trade-off between hover and forward flight efficiency. Fig. 1 plots a number of VTOL concepts in based on their hovering efficiency (disk loading) and cruise efficiency (lift-to-drag ratio).

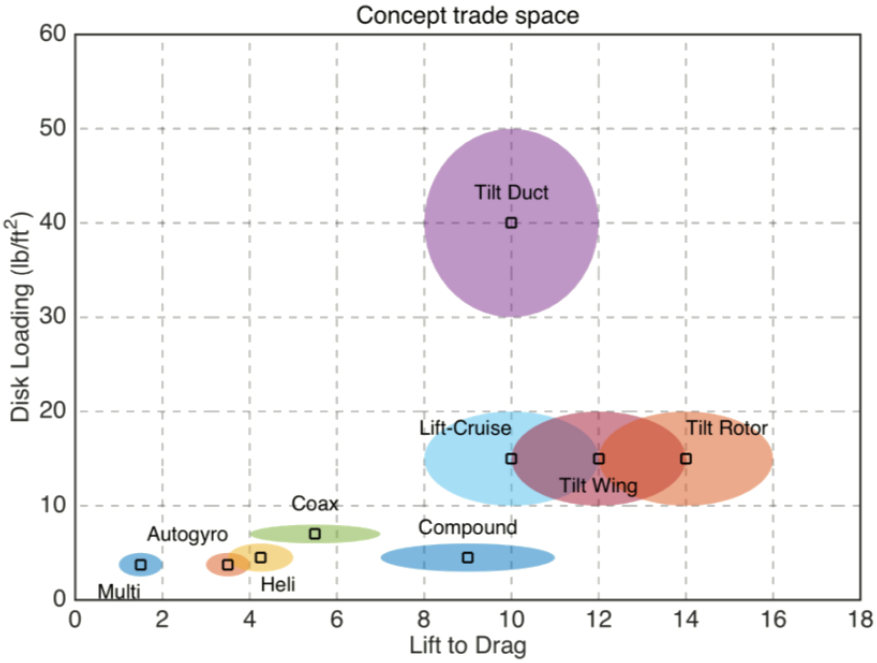

Figure 1 VTOL concept design space [4]

Traditional rotor-driven VTOL aircraft such as helicopters can hover very efficiently, but suffer a massive drag penalty in forward flight due to advancing blade compressibility effects and retreating blade dynamic stall. Extensions or modifications of the traditional helicopter, such as coaxial or compound helicopters, mildly improve the lift-to-drag ratio while suffering only a small penalty in terms of disk loading.

In order to achieve lift-to-drag ratios necessary to enable efficient cruise, which is critical to the feasibility of an electrical UAM or USAM vehicle, more exotic transitioning concepts, such as tilt-wings, tilt-rotors, or tilt-ducts, may be used. However, even the most optimistic tilt-rotor designs struggle to achieve a lift-to-drag ratio greater than 16, which is significantly lower than modern commercial airlines. Additionally, these advanced rotorcraft concepts are far less proven than conventional helicopters and fixed wing aircraft and their complexity may be challenging for cost-efficient operations, safety, and certification.

Additionally, VTOL concepts suffer from rapidly fluctuating power requirements over the course of the mission. During takeoff, hover, and landing, a VTOL aircraft typically consumes over twice the power that is required in cruise. This penalty is felt most heavily by electrical VTOL designs, whose batteries grow less efficient at a higher power output. The need to hover and land vertically drives the sizing of the battery and motor and ultimately the overall feasibility of the vehicle. VTOL aircraft are also acutely sensitive to hover margin requirements, which introduces another unknown into the design process.

Finally, VTOL aircraft produce significantly more noise than their fixed-wing counterparts. The high rotor tip speed, acoustic interactions between rotors, and high downwash velocities of transitioning VTOL concepts all contribute to environmental degradation and disruption. Several key technologies such as distributed electric propulsion promise to reduce the acoustic impact of VTOL vehicles [7], but significant efforts will still be required to keep the noise levels within acceptable limits for a populated area. Potential increased noise regulations could endanger the viability of a VTOL concept altogether.

B. Exploring STOL Potential

STOL or SSTOL aircraft could overcome a number of the aforementioned VTOL deficiencies and potentially integrate into a suburban environment nearly as well as VTOL aircraft. The obvious, and most important, advantage is cruising efficiency. A STOL aircraft's fixed wing is not subject to the same forward flight inefficiencies as a rotary wing and the vehicle can thus carry the same payload further for less energy. No complex and heavy tilting hardware is required to achieve efficiency in both forward flight and takeoff/landing as a STOL aircraft can use high-lift devices (such as slats, flaps, or distributed propulsion) to both takeoff and land at exceptionally slow speeds and cruise efficiently.

Fixed-wing architectures typically require less power for takeoff than a VTOL aircraft, which improves the power balance of the vehicle. Propulsion systems sized for takeoff will not be massively overpowered for cruise, as they generally are on VTOL aircraft, thus reducing the vehicle's empty weight and energy consumption.

STOL aircraft have a lower total noise output than VTOL aircraft assuming similar flight paths. This will significantly reduce one of the primary barriers to operation of an ODM system in an urban or suburban environment by increasing public acceptance of the system. The efficacy of an ODM system would indeed be reduced if all the customers it is meant to serve were to be driven away by noise.

Finally, a STOL concept may be simpler mechanically and less dependent on the development of efficient batteries than a VTOL aircraft. Sizing studies [4] suggest that a minimum of 300 Wh/kg specific energy is required to enable a VTOL aircraft with only 55 nmi of range. Because STOL concepts may be less sensitive to specific energy, it is likely that a functional prototype STOL vehicle could be built sooner than its VTOL cousin.

However, an STOL ODM system has some less desirable aspects. The primary disadvantage is a greatly increased ground footprint compared to VTOL aircraft. Even SSTOL aircraft will likely require a runway of a few hundred feet. Lack of available undeveloped space, especially near urban centers and metro areas where an ODM system would be most in demand, will likely be the greatest challenge for system designers to overcome.

Additionally, STOL aircraft have not been historically as popular as CTOL or even VTOL aircraft. Over the past two decades, only six new STOL aircraft have entered production, and of these six only two were built with passenger transport in mind [8–13]. The increasing number of large, well-developed airports has relegated STOL aircraft into niche markets such as bush flying, recreational vehicles, and utility aircraft. A lack of suitable baseline STOL vehicles built for commercial transportation might make the development of an ODM STOL system more difficult.

II. Approach

This paper explores the effects and implications of the takeoff and landing runway length requirement for STOL ODM operations. As the field length requirement is reduced, more airparks could likely be built in a given area, thus increasing the airpark geo-density and potentially reducing travel time. It is hypothesized that a certain minimum airpark geo-density in a given region will allow STOL aircraft to be as capable as or more capable than VTOL aircraft for an ODM application.

Traditional airport design approaches take a substantial amount of time to complete and involve numerous studies, reports, assessments, and negotiations. Because an aerial ODM system is likely to require hundreds or even thousands of airparks to effectively serve a metropolitan region, a simple, rapid process is required to estimate the maximum airpark geo-density possible in a city so as to assess system feasibility in the early stages of the system design process. Additionally, this process must be fully agnostic to any specific vehicle concept to allow sufficient design freedom.

The process begins by selecting a candidate city for study. Next, the city's land use regulations are examined and a number of parametric airpark concepts are placed and sized in suitable locations, thus allowing a calculation of airpark geo-density. By modifying vehicle performance and airpark sizing parameters, we can rapidly analyze the sensitivity of airpark geo-density to a number of different factors. These sensitivity studies can ultimately be used to help define appropriate requirements for STOL vehicles serving in an ODM system.

A. Candidate Cities

For the purposes of this report, a single candidate metropolitan area is selected. However, all of the methods and tools developed are applicable to any city worldwide. While selecting a suitable candidate city, a number of different parameters are considered to establish feasibility.

The primary requirement for any STOL system is ample suitable space to build a significant number of airparks. Thus, cities with extremely high density and infill, such as New York City, would be less favorable. Highly dense cities are typically the result of their position in an area-constrained location. For example, the extreme density on Manhattan is driven by the need to build upwards and inwards, rather than outwards, as the city grows.

Metropolitan areas surrounding a city center are typically much less dense and may be suitable for ODM operations. However, a city that is less dense overall, such as Atlanta or Dallas–Ft. Worth, would be more desirable. These types of cities are characterized by their position in a non-area-constrained location. Cities such as Atlanta and Dallas are relatively free to expand radially away from the city center, which is generally less costly than vertical or infill development. As a result, these cities tend to have larger numbers of vacant or nearly-vacant spaces in their most dense regions. The open space requirement also favors cities with significant amounts of undeveloped land, such as greenfields (undeveloped land with no contamination) or brownfields (undeveloped lands deemed too contaminated for residential development.) Brownfields tend to be more prevalent in cities with strong industrial histories [14], such as Rochester or Detroit.

Finally, water features such as lakes, rivers, or oceans present additional landing sites in the form of barge-based airparks. Placing airparks on barges will allow the system to serve exceptionally dense regions of cities typically found along waterfronts. Due to the high value of land in these areas, it is unlikely that any vacant dry ground will be available for purchase. Thus, an ODM aerial system will need to develop innovative new airpark technologies to serve all of its potential customers.

It is also important to consider the existing state of the transportation network in a city. A candidate metropolitan region's primary transportation network must allow and encourage aerial ODM operations. Thus, we are primarily interested in cities with a significant amount of automobile-based traffic congestion, as revolutionary automobile alternatives could benefit these cities more substantially than a city with a large and efficient public preexisting transportation system. ODM operations are also benefited by the presence of at least one large commercial airport and several smaller general aviation airports, as these facilities serve as links to thin-, medium-, or long-haul aviation routes and effectively expand the reach and utility of the ODM aerial system.

A city's climate also has a significant impact on its suitability for a prototype ODM STOL system. Although this system will ultimately need to be able to operate in reduced visibility, high surface winds, and icy conditions, a city with relatively calm and consistent weather patterns would be an ideal testing ground as the safety, automation, and robustness of the system design is improved.

Because the initial operating costs of an ODM system will be high, we must select a city that has a relatively wealthy population. Wealthy residents will more easily accept the high early adopter costs of ODM transportation and will enable system testing, validation, and optimization before the system is deployed to other metropolitan areas at a lower cost. Additionally, companies in the high tech industry may be more willing to invest in revolutionary concepts, which will further reduce the barrier to entry. As such, we also considered cities that serve as tech industry hubs in their respective regions.

A number of cities were surveyed with the aforementioned parameters in mind. Ultimately, nine were shortlisted for more detailed study. Many of the cities included have been previously referenced in other studies as potential candidates for ODM and UAV implementation [1, 6]. The results were organized into a Pugh matrix in Table 1, where a (+) indicates an advantage in a certain parameter, a (−) indicates a disadvantage, and a (∘) indicates neither an advantage nor a disadvantage. Note that city names in Table 1 refer to an entire metropolitan area, not just the city itself. For example, "New York City" would refer to the entire NY–NJ–CT tri-state area rather than simply the legal boundaries of NYC.

Ultimately, Miami and Dallas–Ft. Worth emerged as the top options in the candidate city study. However, we found that geographic information data for many counties surrounding the Dallas–Ft. Worth area was restricted, so Miami was ultimately selected as the primary region of interest while developing this tool. A number of other cities, including Los Angeles, Atlanta, and Silicon Valley also show strong potential and could be used as additional case studies for future work related to this research.

For the purposes of this research, the Miami metro region refers to the combined area of Miami-Dade, Broward, and West Palm Beach counties, and includes the cities of Miami, Ft. Lauderdale, and West Palm Beach, as seen in Figure 2. This area spans over 6,000 square miles in the south-east corner of the state of Florida and is home to over six million residents. The large sprawl and high commute times between Miami and West Palm Beach; the ample number of nearby water bodies such as the Intercoastal Waterway, Lake Okeechobee, and many smaller rivers and lakes; the higher-than-average wealth of many of the residents; the relatively mild climate; and the rapidly evolving high-tech industry in Miami all serve to make it an ideal candidate for the development of a STOL ODM transportation system.

Table 1 Comparison of candidate metropolitan areas

Metro region	Wide sprawl	Appropriate density	Water bodies	Population wealth	High-tech industry	Congestion	Pre-existing airports	Weather	Advantages	Disadvantages	Neutrals	Total
Miami	+	+	+	+	○	+	+	○	6	0	2	6
Dallas–Ft. Worth	+	+	+	+	+	○	+	○	6	0	2	6
Los Angeles	+	○	○	+	○	+	+	+	5	0	3	5
Atlanta	+	+	−	+	+	○	+	○	5	1	2	4
Silicon Valley	−	○	+	+	+	+	+	○	5	1	2	4
Houston	+	+	○	+	○	+	○	○	4	0	4	4
New York City	+	−	+	+	+	+	○	−	5	2	1	3
Boston	○	○	+	○	○	+	+	−	3	1	4	2
Chicago	○	○	+	○	+	○	+	−	3	1	4	2

Figure 2 Counties in southern Florida [15]

B. Airpark Concepts

After selecting our metropolitan region, we developed a number of realistic, parametric, resizeable airpark concepts to fit within the metropolitan region itself. The primary purpose of this portion of the process is to enable a realistic solution for the actual airpark geo-density calculation, which will be discussed in the following section of this paper.

The size and location of an airpark is influenced by a number of core factors [16]. The first and most obvious is the runway length, which is directly dependent on the takeoff performance of the vehicle in question. The balanced field length (BFL) of a given vehicle was used to size the runway to ensure safe takeoff abort ability in a one-engine-inoperative (OEI) situation. However, in addition to the runway, associated infrastructure such as the threshold, taxiway, ramp, public safety areas, aircraft charging and storage locations, and pickup/drop-off points for automobile transport increase the size of the airpark. Innovative airpark designs are necessary to reduce the overall airpark footprint to a manageable level.

The size and position of an airpark is also influenced by its interactions with its environment. An airpark must be

sized and positioned correctly to allow vehicles to clear nearby obstacles during departure and approach. Additionally, the local atmospheric and weather conditions in a region also influence airpark size and position. Icy or snowy conditions require runways to be longer than normal to accommodate decreased braking force during landing. Wind magnitude and direction can force runways into a specific orientation, and the atmospheric impact on noise propagation may require airparks to grow to contain their noise footprint. Due to the preliminary nature of this analysis, the impacts of atmospheric and weather conditions were not considered for this paper.

We developed three airpark concepts to fit a variety of potential locations: the standard concept, the reduced width concept, and the barge concept. In order to ensure the realism of these concepts, we applied appropriate FAA design recommendations, listed in FAA AC 150/5300-13A, to the airpark concepts. We assumed that vehicles using these airparks would fall into aircraft approach category I, airplane design group I, and taxiway design group I, which generally encompass all aircraft having an approach speed of less than 91 knots, a tail height of less than 20 feet, and a wingspan of less than 49 feet.

The resulting applicable safety recommendations include a runway width of 60 feet including safety margin and a taxiway width of 49 feet including safety margin. The FAA also recommends a runway safety area of 600 feet on either end of the runway for group I aircraft; this constraint would severely impact STOL ODM system feasibility. Thus, we created a runway safety length parameter R to study the sensitivity of geo-density to different potential runway safety area requirements. Finally, we generalized the recommend parking space area to derive an equation for parking space side length as a function of aircraft wingspan. Using the maximum possible group 1 wingspan of 49 feet, we determined each parking spot should have a side length of 59.8 feet.

Certain structures were not included in the airpark design to reduce complexity. We assumed that all customers using the STOL ODM system would arrive at the airpark using a rideshare service. Thus, airparks do not include long-term parking spaces for automobiles. However, the addition of a small number of automobile waiting spaces into the concept would not dramatically alter its overall size. Additionally, we assumed that the majority of airpark logistical operations would be decentralized or automated. Thus, these concepts do not include administrative or other facility buildings. Finally, we assumed that infrastructure necessary to charge or swap out the vehicles' batteries would not be significantly large enough to require their own dedicated space.

Figure 3 Standard airpark concept design.

The standard airpark concept, portrayed in Fig. 3, consists simply of a runway, an adjacent taxiway, and parking spaces to allow pickup and drop-off locations for users of the system. The bounding box describing this airpark concept has a length of $L + 2R$ feet and width of $109 + S$ feet, where L is the runway length, R is the previously-defined runway safety area parameter, and S is the parking lot side length.

The narrow concept, presented in Fig. 4 differs from the standard concept in that the taxiway is removed, leaving only a runway alongside some parking spaces. This reduces the width of the concept by nearly 50 feet, allowing the airpark to fit in extremely narrow plots of land such as in greenspace alongside highways. However, the lack of a separate taxiway implies that some vehicles will need to taxi down the runway to reach the proper spot, thus reducing overall throughput. Although throughput calculations were not considered at this stage, we were interested in determining the potential increase in geo-density that could gained by switching to this concept design when necessary. The bounding box of the narrow concept has a maximum length of $L + 2R$ feet and a maximum width of $60 + S$ feet.

The barge concept, seen in Fig. 5 allows us to place airparks in areas where vacant land space is limited, such as nearly highly valuable waterfront locations alongside rivers or near a beach. Soft concrete is placed at either end of the

Figure 4 Reduced width airpark concept design.

Figure 5 Barge airpark concept design.

runway to prevent potential runway overruns. The barge integrates with a small patch of vacant land onshore through the use of a vehicle ramp, which could either allow automobiles to drive onto the barge and meet passengers or allow the STOL aircraft to taxi onto shore to meet automobiles. The bounding box dimensions of this concept are identical to those of the narrow airpark.

C. Airpark Construction Types

Each airpark concept requires associated placement rules to map it to a suitable location in the Miami metropolitan region. These rules took the form of four different airpark construction types, each of which is correlated with one or more of the previously discussed airpark concepts.

The first construction type is *vacant land construction*. This type specifies all land that is considered to be vacant by its governing county and includes land with abandoned and unused structures. However, certain tracts of land have been set aside conservation or water management purposes, such as those in the Florida Everglades. Such regions were intentionally excluded from consideration in this analysis. The vacant land construction type can be fulfilled by standard or narrow airpark concepts.

The second construction type is the *barge construction type*, which correlates with the barge airpark concept. The primary requirement for this construction type is simply a usable, suitably large water body, such as a river or lake, the Atlantic Ocean, or the Intracoastal Waterway. Certain types of water body, such as those used for irrigation supply or residential boat basins, were excluded from this process. However, because the barge must integrate with onshore infrastructure, we selected small regions of vacant land adjacent to these water bodies to serve as the actual "location" of these airparks. The piece of land represents the interface between the barge and the on-shore infrastructure, and the barge itself occupies the associated water body.

The third construction type is *additive construction*. This construction type describes airparks built on large surface parking lots or parking decks, which could potentially increase geo-density beyond what vacant land and barges may

offer, especially in denser downtown areas. However, additional operational, legal, and business considerations will be required to enable this type of airpark construction, which were not considered for this study.

The final construction type is *pre-existing airparks*. We assumed that all active and inactive airports in the Miami region could be incorporated into our system as airparks. This also includes a number of private aerodromes which serve small communities in the region. However, we specifically excluded military and private commercial airports such as the Sikorsky facility in West Palm Beach (06FA) under the assumption that it would not be possible to purchase these facilities.

D. Airpark Placement

The next step in the process is to select a number of suitable airpark locations based on the previously defined construction types and concepts. This process was accomplished by collecting data describing the land use classification of each parcel in the county of interest, which was distributed by the Florida Department of Revenue (DOR) [17].

Land use regulations divide a county into a large number (typically several hundreds of thousands) of land parcels, each which is classified according to a different land use code, which governs acceptable uses for the land. Classifications include residential, commercial, industrial, agricultural, preserve, vacant, and many more. Land use differs from zoning laws in that land use is typically more general and used primarily for future planning purposes; zoning laws specify more detailed regulations such as building setback, maximum height, and architectural style, and are thus less appropriate for this application.

Land use definitions are distributed by the Florida DOR in the form of geographic information system (GIS) datasets, which essentially act as interactive maps with layers and tags to allow detailed filtering. We combined, filtered, and transformed this data using Quantum GIS (QGIS), a free GIS software package, to identify parcels matching each of the four construction types and export their data for further processing.

Each airpark construction type was converted into a series of QGIS operations to automatically select and extract parcels meeting the construction requirements. In the case of the vacant land construction type, a simple boolean filter was used to identify parcels designated as "vacant" by the Florida Department of Revenue. Parcels under 48,000 square feet were filtered out to minimize the number of extremely small parcels in the dataset.

For the barge construction type, two boolean filters were used to create a set of vacant land parcel and a set of usable water bodies. A 100-foot buffer was placed on the water body set so as to capture adjacent parcels. The spatial intersection of these two sets forms a set of vacant land parcels that can serve as the water/land interface component of the barge airpark concept. The barges themselves were fit within the lake and later associated with the onshore parcel thus allowing a single large lake to contain multiple barges at different places along the shore.

To identify large parking decks for the additive construction type, we collated a list of malls, large retailers, and other buildings with large surface lots in the region of interest, retrieved their GPS coordinates from Google Earth, and extracted associated land parcels. However, it was infeasible to determine which fraction of a given parcel was occupied by the building and which fraction was occupied by a parking lot. Based on a survey of satellite images of several large retailers in the Miami area, we made the assumption that approximately 50% of the area in a given parcel would be associated with a parking deck, leading to the assumption that the maximum true runway length of an additive-construction-type airpark is half that of a vacant-land-type airpark in an identical parcel.

Data for the pre-existing airpark construction type was collected from the FAA, which reports GPS coordinates and runway length for every identified airport or airstrip in the area. In cases with multiple runways, the longest runway was used to represent the airpark.

We then developed a method to easily exclude potential airpark locations that are too close to a large obstacle for safe operation. Obstacles are a concern for any airport, but become especially important for airports in urban and suburban environments. Because the orientation of the runway and the climb performance of the vehicle are unknown at this point in the process, we adopted a conservative approach that would assume the worst possible case for obstacle interactions.

Data for all significant obstacles in the region was obtained from the FAA Obstacle Data Team's database. This database documents over 7,000 obstacles in our three counties of interest, listing each obstacle's height above ground level alongside exact GPS coordinates. However, this database may not adequately document obstacles that are shorter than 200 feet and also not located near any preexisting airports. However, as this is the best obstacle data available at the time of writing, we had to proceed with this limitation in mind.

The impact of each obstacle on nearby airparks was assessed by defining an obstacle's exclusion radius, r_e, as described in Fig. 6. The exclusion radius equation is derived by determining the horizontal distance necessary to clear an obstacle adjacent to the airport after crossing over the runway threshold.

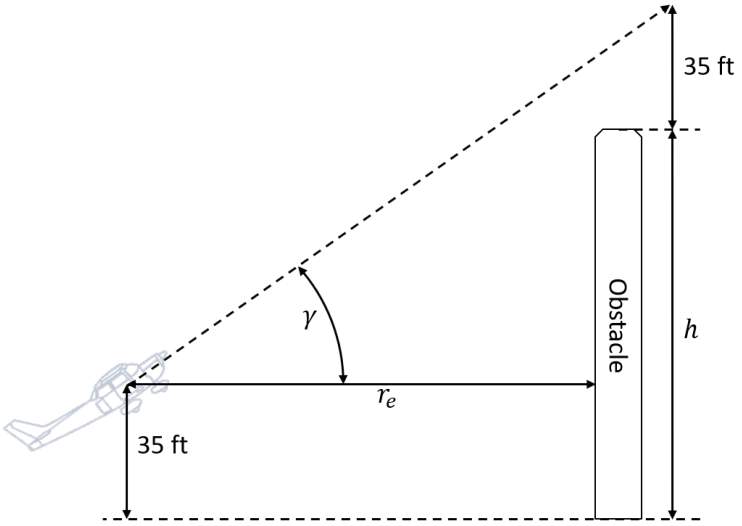

Figure 6 Exclusion radius equation formulation.

For the purpose of these calculations, we assumed that the airpark's runway would be sized such that a vehicle would be capable of reaching at least the conventional 35 feet altitude by the end of the runway. In order to reflect the most conservative scenario, we also assumed that the end of the runway would run directly to the edge of a given parcel and that the vehicle would fly directly towards the obstacle at a flight path angle γ and need to pass over it with another 35 feet of clearance.

Thus, we define the exclusion radius equation as

$$r_e = \frac{(h + 35) - 35}{tan(\gamma)} \tag{1}$$

where γ is the climb angle, h is the obstacle height above ground level, and r_e is the exclusion radius. We assumed that all vehicles used in this system would be high performance STOL aircraft capable of climbing at an angle of roughly 15 degrees, thus simplifying the equation to

$$r_e \approx 3.732h \tag{2}$$

All airpark parcels of the vacant land and additive construction types intersecting an obstacle exclusion radius were removed from consideration. Ultimately, this ended up removing approximately 14% of the total airparks in the region, which suggests that the impact of obstacles may not be as constraining as we initially assumed. The sensitivity of this method to the climb angle assumption was assessed by repeating the process for other values of γ. These results are presented in Table 2.

Table 2 Sensitivity of obstacle assessment method to climb angle assumption

γ (°)	Airparks removed (%)
10	19.20
15	13.57
20	11.37

Based on Table 2, increasing the climb angle assumption beyond 15° does not have a strong effect. However, a lower climb angle assumption decreases the number of airparks available significantly. For context, commercial aircraft such as the Boeing 737 can typically climb at 15–16° just after takeoff, and general aviation aircraft typically climb around 5–10° [18]. To avoid significant airpark geo-density penalties due to obstacle interactions, ODM STOL vehicle designers must strive to at least match the takeoff performance of conventional airliners.

A sequence of images demonstrating the airpark filtering process for a portion of the Miami metropolitan region is presented in Fig. 7. Although this paper focused only on Miami-Dade, Broward, and Palm Beach counties, this process

is easily expandable to other counties in Florida using additional land use data distributed by the Florida DOR. The process could also be extended to counties in other states, although some modifications would likely need to be made to reflect differing land use codes and data distribution methods.

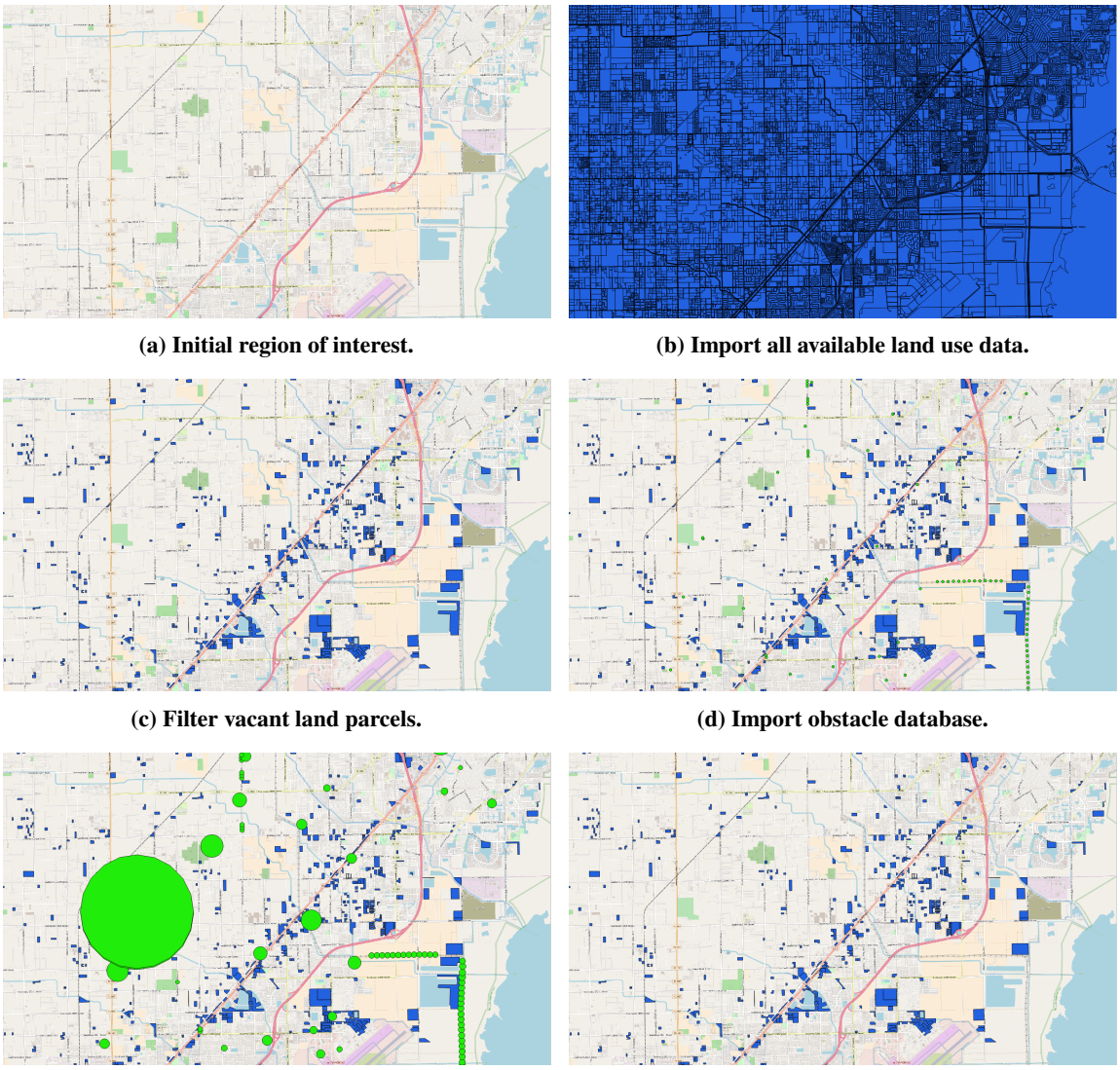

(a) Initial region of interest.

(b) Import all available land use data.

(c) Filter vacant land parcels.

(d) Import obstacle database.

(e) Apply obstacle exclusion radius equation.

(f) Remove intersecting parcels.

Figure 7 Demonstration of airpark parcel selection process.

E. Airpark Fitting

Given the filtered parcels available to place airparks in, the next step is to figure out what size airpark fits in each of these parcels. In general, the parcels are arbitrary polygons with the vertices defined by the nodes previously recorded. No assumptions can be made about the number of vertices or their relative arrangement. In the simplest cases, parcels may be rectangular, with four vertices with relatively equal angles between them; in other cases, the parcels may have many more vertices and non-convex geometries. The problem of fitting rectangles into polygons has been explored previously [19]. The usual formulation focuses on maximizing the area of the inscribed rectangle under a variety of constraints. For the airpark fitting problem, no assumptions may be made as to the convexity nor the alignment of the rectangle. The approximate approach presented by Molano et al. for “finding the largest area rectangle of arbitrary orientation in a closed contour" [20] in $O(n^3)$ time meets these requirements, but relies on producing a quasi-lattice

polygon inscribed inside the contour. The D3plus javascript library for data visualization has an alternate approximate largest rectangle algorithm for the purpose of fitting data labels inside stacked area charts. While this second approach does not give guarantees on accuracy or time complexity, it is well documented [21] and the source code is accessible on GitHub. For the sake of portability, this open source method was translated into Python. Additionally, the algorithm was modified to fit the problem at hand: in the case of airpark fitting the rectangle of interest is not the one with the largest area, but the longest rectangle of a given width. Thus, simplifications can be made by removing logic relating to calculating and comparing the area while still preserving the underlying scheme. The method used is shown in Algorithm 1.

Algorithm 1 Find the length l_{max} of the approximate longest rectangle of width w in a polygon P

function LONGEST_RECT($P, w, \alpha, n, l_{step}$)
  $l_{max} \leftarrow 0$
  for $O_i \in \{O_1, \ldots, O_n | O_i \text{ inside } P\}$ **do** ▷ For n randomly selected origins inside P
    for $\alpha_i \in \alpha$ **do** ▷ For each heading in given range
      $p_{11}, p_{12} \leftarrow intersection(P, \text{ ray through } O_i \text{ along } \alpha_i)$
      $p_{21}, p_{22} \leftarrow intersection(P, \text{ ray through } O_i \text{ along } \alpha_i + \pi/2)$
      $O'_{i_1} \leftarrow midpoint(p_{11}, p_{12})$
      $O'_{i_2} \leftarrow midpoint(p_{21}, p_{22})$
      for $O'_{ij} \in \{O_{i_1}, O_{i_2}\}$ **do** ▷ For each modified origin
        $p'_{11}, p'_{12} \leftarrow intersection(P, \text{ ray through } o'_{ij} \text{ along } \alpha_i)$
        $p'_{21}, p'_{22} \leftarrow intersection(P, \text{ ray through } o'_{ij} \text{ along } \alpha_i + \pi/2)$
        $l_{max_{O'_{ij}}} \leftarrow 2 \times min(length(O'_{ij},\ p'_{11}), length(O'_{ij},\ p'_{12}))$ ▷ Compare lengths of each ray
        $w_{max_{O'_{ij}}} \leftarrow 2 \times min(length(O'_{ij},\ p'_{21}), length(O'_{ij},\ p'_{22}))$
        if $\left(w_{max_{O'_{ij}}} \geq w\right) \wedge \left(l_{max_{O'_{ij}}} > l_{max}\right)$ **then** ▷ If width, length satisfied along $\alpha_i + \pi/2, \alpha_i$
          $l_{lower} \leftarrow l_{max}$
          $l_{upper} \leftarrow l_{max_{O'_{ij}}}$
          while $\left(l_{upper} - l_{lower}\right) \geq l_{step}$ **do**
            $l \leftarrow \left(l_{lower} + l_{upper}\right)/2$
            if rectangle(O'_{ij}, l, w) fits in P **then** ▷ Rectangle centered on O'_{ij}, length l, width w
              $l_{max} \leftarrow l$
              $l_{lower} \leftarrow l$
            end if
            $l_{upper} \leftarrow l$
          end while
        end if
      end for
    end for
  end for
  return l_{max}
end function

The function requires as inputs the polygon P representing the parcel of land, the width w of the airpark, the range of heading angles α to consider, the number n of random origin points to use when placing the rectangles, and the binary search minimum step size l_{step}. The original randomly selected center points O inside the polygon may be close to the edges and in these cases rectangles centered on them would likely not be the largest rectangles that can be fit. To remedy this, modified origin points O' that lie more towards the interior of the polygon are generated from each original point. To generate these better center points, rays are cast along the length direction α_i and the perpendicular width direction $\alpha_i + \pi/2$. For each ray, the new O' lies at the midpoint between the first intersection of the ray and the polygon, to either side of the original O. At each O' rays are again cast along α_i and $\alpha_i + \pi/2$, and the distances between first intersections and the origin O' recorded.

Because O' defines the center point of the potential rectangle, the tentative maximum length that can be fit in this origin is twice the shortest distance from O' to the polygon along α_i and the tentative maximum width that can be fit is

twice the shortest distance from O' to the polygon along $\alpha_i + \pi/2$. The polygon may still impinge on a rectangle of these maximal dimensions, but if these tentative values do not satisfy the width requirement or do not exceed the current best length, the origin can be rejected at this α_i outright. If however they are met, the longest rectangle that fits inside the polygon with width w and the long direction aligned with α_i is found using a binary search method. The length is initialized as the mean of the current best length and the tentative maximum length, and a rectangle generated. If this rectangle fits inside the polygon, a new best length has been found and the lower bound is set to the length of the rectangle. If this rectangle does not fit inside the polygon, the upper bound is set to the length of the rectangle. This process is repeated until the new length generated as the mean of the lower and upper bound is less than the minimum step size l_{step}. The entire scheme is repeated for all the original origins O at each angle in the range of angles α. A simplified illustration of this process for a single O' and α_i is presented in Fig. 8.

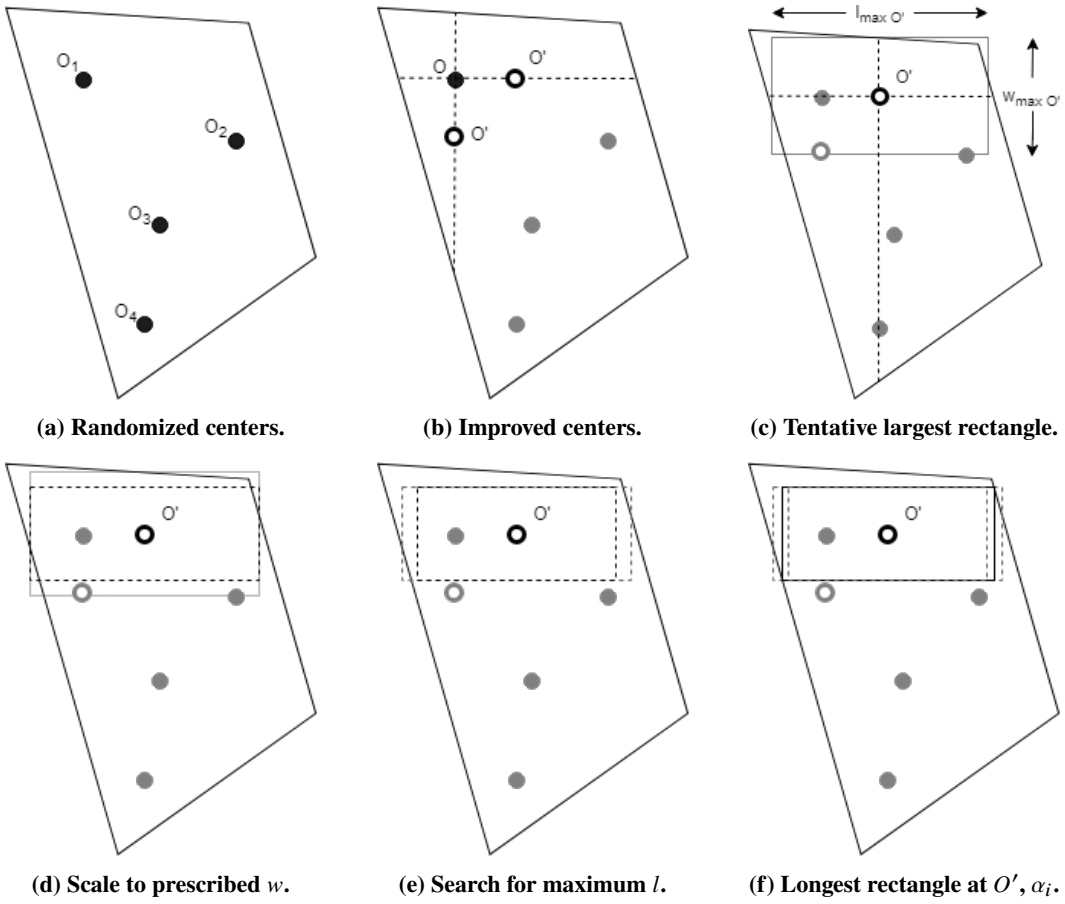

(a) Randomized centers. **(b) Improved centers.** **(c) Tentative largest rectangle.**

(d) Scale to prescribed w. **(e) Search for maximum l.** **(f) Longest rectangle at O', α_i.**

Figure 8 Illustration of rectangle fitting algorithm for single O' and α_i.

This algorithm was implemented in Python 3 and made use of the `Polygon` library which provides utilities such as polygon intersection checking and generation of visualizations for debugging and sanity checking purposes. The script was run on preprocessed data files containing the vertices of the filtered parcels. The longest inscribed rectangle in each parcel was then returned and associated with the specific parcel identification number. The process was repeated for $w = 119.8$ feet and $w = 168.8$ fee to account for the differing widths of the airpark concepts, based on the standard and narrow width concepts discussed in Sec. IIB. Angles were varied in the range $[-90, 90]$ in increments of 2 degrees. The number of original origins was $n = 20$, and l_{step} is defined as 2% of the smaller dimension of the bounding box of the polygon. With these parameters, the runtime for a single parcel was ~0.1 to 0.5 seconds, depending on the number of vertices in the polygon. Running the script over night allowed the entire dataset to be processed with minimal hassle in a few days.

To verify the success of the algorithm in finding approximate largest rectangles for a variety of parcel shapes, visualization of the largest inscribed rectangles in each parcel were generated and inspected. Figure 9 shows some

examples, demonstrating that the script is able to find the approximate largest rectangles as desired, even for parcels with complex shapes. The dark blue shape represents the parcel, while the light blue rectangle represents the longest inscribed rectangle found by the algorithm. The dots inside the parcel show the locations of origins and modified origins at which the algorithm centered rectangles during the search.

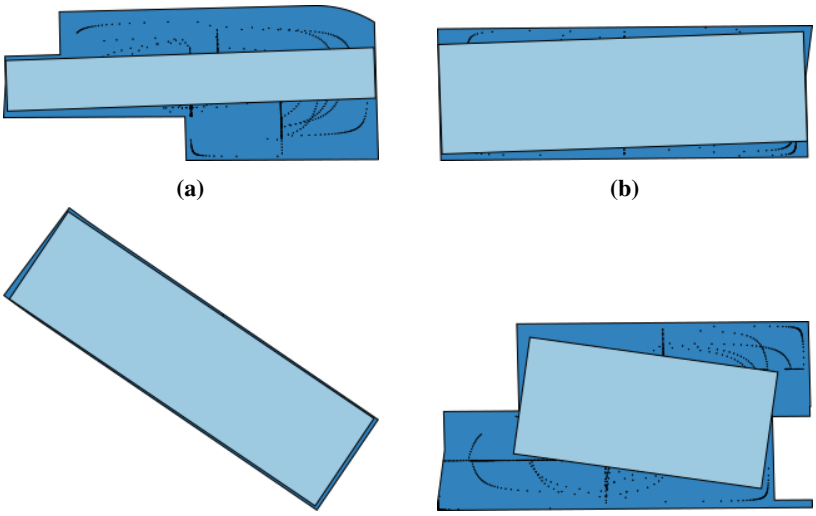

(a) **(b)** **(c)** **(d)**

Figure 9 Well fit rectangles of fixed width.

However, sometimes the algorithm's result was determined to be less than ideal. This is to be expected as the algorithm is stochastic and only provides approximate solutions. Examples are shown in Fig. 10. The predominant failure mode is an angle misalignment, in which the parcel is close to rectangular, with the short side length just slightly larger than the rectangle width and the long principal axis at an angle which is not one of the discrete steps in the angle sweep range. Because the algorithm only attempts to fit rectangles along the specified α heading angles, if the length of the rectangle depends strongly on precise alignment with a specific angle and this angle is not explicitly included, the true longest rectangle cannot be found. If the width of the parcel is almost exactly the required width and the margin for misalignment minimized, this can lead to results that are considerably shorter than the true longest rectangle. A second, more uncommon failure mode stems from the random generation of origins and the assumption that better origins lie at the midpoint of rays cast from these original random origins. While in most cases, this technique for generating modified origins results in center points that lead to maximum length rectangles, in some complex parcel geometries the ideal point cannot be not identified. This leads to rectangles that have the correct alignment, but, because their center point is on the midpoint of a ray instead of in the middle of what can be visually identified as the "free" space, do not have the true maximum length for the parcel. Fortunately, this type of suboptimal result is rare because parcels with the complex geometry that causes this issue are uncommon. Both of these limitations of the algorithm can be mitigated and the approximate solution improved at the cost of increased computational time by increasing the angle sweep resolution and the number of original random origins, respectively.

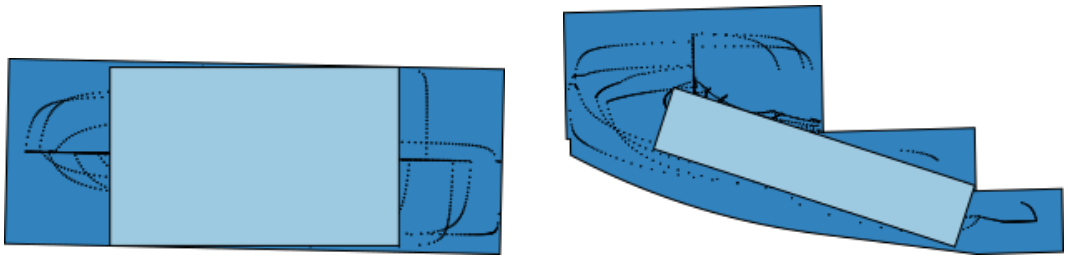

(a) Angle misalignment **(b) Poor origin placement**

Figure 10 Algorithm limitations.

Inspecting the results visually also highlights the benefit of the narrow-width airpark concept. In many cases where parcels are not wide enough to accommodate full-width airparks of significant length, the narrow concept can be successfully placed, as shown in Fig. 11. This narrow concept can also mitigate the impact of the angle misalignment case, as the decreased width allows the rectangle to have more margin for misalignment and more of the true maximum length will be recovered by the algorithm.

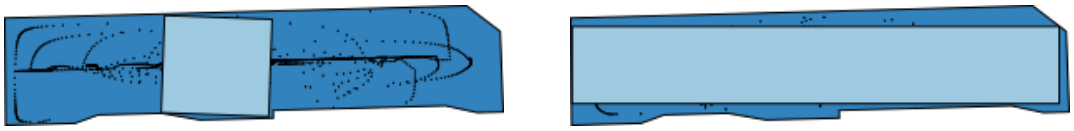

(a) Standard width concept **(b) Narrow width concept**

Figure 11 Effect of airpark width on maximum length.

III. Results and Analysis

The ultimate output of the airpark geo-density process is a dataset describing potential airpark locations in the selected metropolitan region. Each airpark in the dataset is associated with a set of GPS coordinates, the maximum runway length for the primary airpark concept, and the maximum runway length for the alternative airpark concept, if applicable.

In total, the vacant land construction type contains 9,517 potential airpark locations. The barge construction type adds an additional 5,372 locations. The additive construction type adds 763 potential airpark locations, and the preexisting airpark construction type adds another 14 potential airparks for a total of 15,666 potential airpark locations in the Miami metropolitan area. However, these numbers do not consider the impact of STOL vehicle performance in terms of minimum balanced field length.

In order to visualize these results in more detail, we create a cumulative distribution function (CDF) of airparks by maximum available runway length. The CDF describes how the number of available airparks in the candidate city decreases as the runway length requirement increases, and can be used to directly analyze sensitivity of airpark geo-density to vehicle performance parameters.

We can also visualize the results spatially by creating heatmaps of the airpark distribution. Heatmaps provide a qualitative measure of relative airpark geo-density in geographic space, and can be used to analyze the impact of different airpark types and runway length requirements on the spatial distribution of all potential airparks in the area.

A. Visualizing Geo-density

Figure 12a shows the CDF for the vacant land airpark construction type only. The maximum available geo-density using only this construction type is 1.55 airparks per square mile, although this drops drastically as the runway length requirement increases. As the runway length requirement approaches 300 feet, our available geo-density decreases to just 0.97 airparks per square mile, or 62.6% of the maximum, if including the narrow width airpark concept, or only 50.29% if only considering the standard airpark concept. As runway length increases to 600 feet, available geo-density decreases to 0.44 airparks per square mile, or 28.4% of the maximum, if using the narrow width airpark concept, or only 24.9% if only considering the standard airpark concept. As the runway length requirement exceeds 1000 feet, the available geo-density is only a small fraction of the maximum. This sharp decrease in available airpark geo-density highlights the need to create innovative, high-performance STOL vehicles with advanced high-lift devices to make this system practical.

For reference, the Miami metropolitan area is currently served by 14 airports, giving an average geo-density of 2.28×10^{-3} airports per square mile. Thus, nearly all possible scenarios involving STOL airparks offer several-orders-of-magnitude geo-density improvement over the current aerial transportation network.

The CDF also shows that significant advantages can be gained by constructing the narrow width airpark concepts where necessary. In the region between 150 to 250 feet maximum available runway length, approximately 1,100 airparks can be added if using the narrow width concept, correlating to a geo-density increase of approximately 0.18 airparks per square mile.

Figures 12b, 12c, and 12d present heatmaps for the vacant land construction type airpark distribution at zero, 300, and 600 feet maximum available runway length, respectively. In these figures, yellow represents high local relative

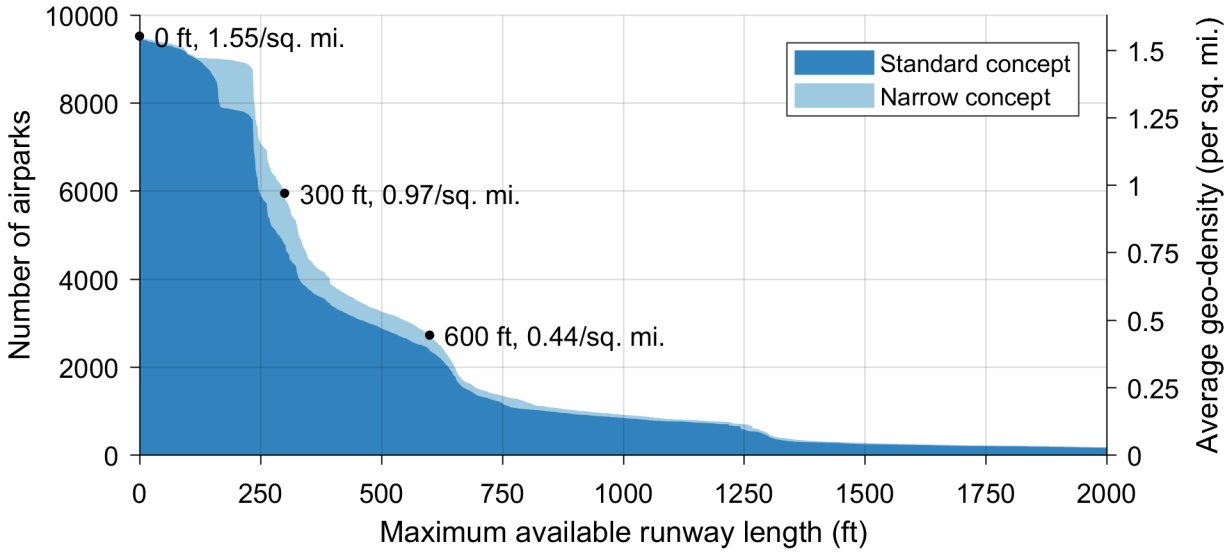

(a) Cumulative distribution function of vacant land construction type.

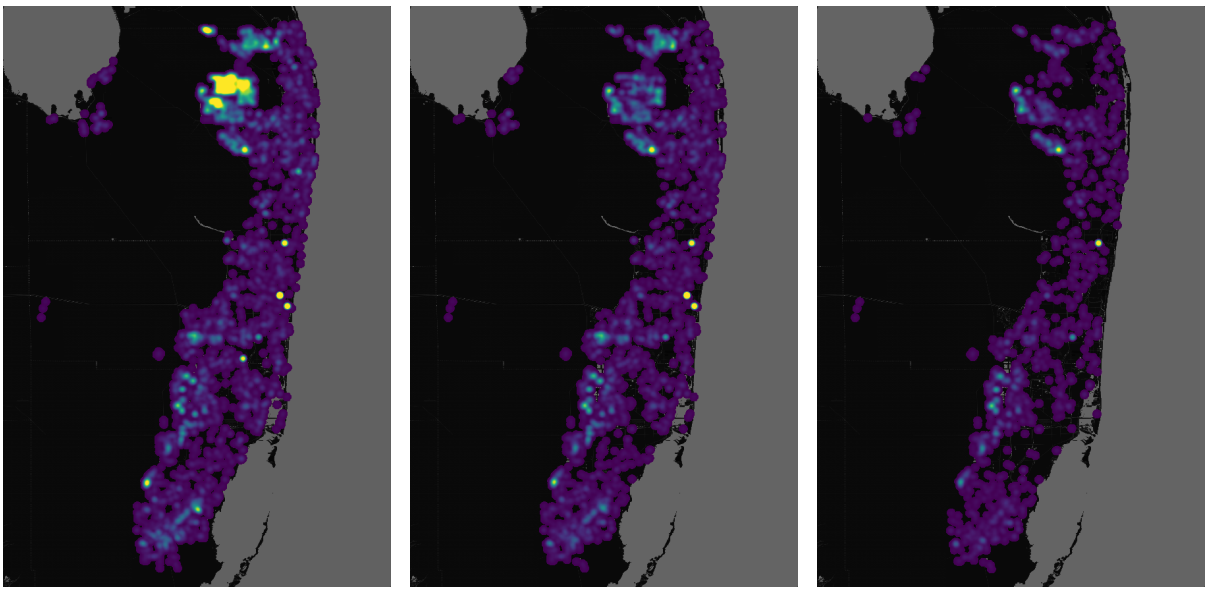

(b) Heatmap with no length limit. **(c) Heatmap at 300 ft length limit.** **(d) Heatmap at 600 ft length limit.**

Figure 12 Geo-density analysis of vacant land construction type.

geo-density and purple represents low local relative geo-density.

In Fig. 12b, we can see that airparks are relatively evenly distributed across the three counties of interest. However, there are a number of hot spots of high local relative geo-density on the map. Primarily, we can see an extremely high local relative geo-density just north of West Palm Beach, which represents a lightly developed residential neighborhood. Roughly half the parcels in this neighborhood contain structures, and the rest currently exist as undeveloped, heavily wooded lots. Note, however, that these parcels have been sized for single-family developments, and this sizing limits their effectiveness as potential airpark locations. We can see the hotspot's brightness has decreased significantly in Fig. 12c and nearly vanish in Fig. 12d.

Additionally, there is a region of increased local relative geo-density on the west side of Miami-Dade County, where the city meets the Everglades. This region contains a large number of artificial ponds surrounded by vacant lots that are not marked for agricultural or preservation purposes. This region offers an opportunity to serve customers in the city of

Miami that may live in extremely densely-populated regions. Note that the parcels in this region are much larger than in the aforementioned neighborhood; we can see the same bright region in Fig.s 12c and 12d.

However, the vacant land construction type does not serve customers who live in dense regions well. In the more heavily populated eastern and central portions of Miami-Dade county, the relative local geo-density is very thin. This drives a need for additional airpark construction types to serve residents of these regions.

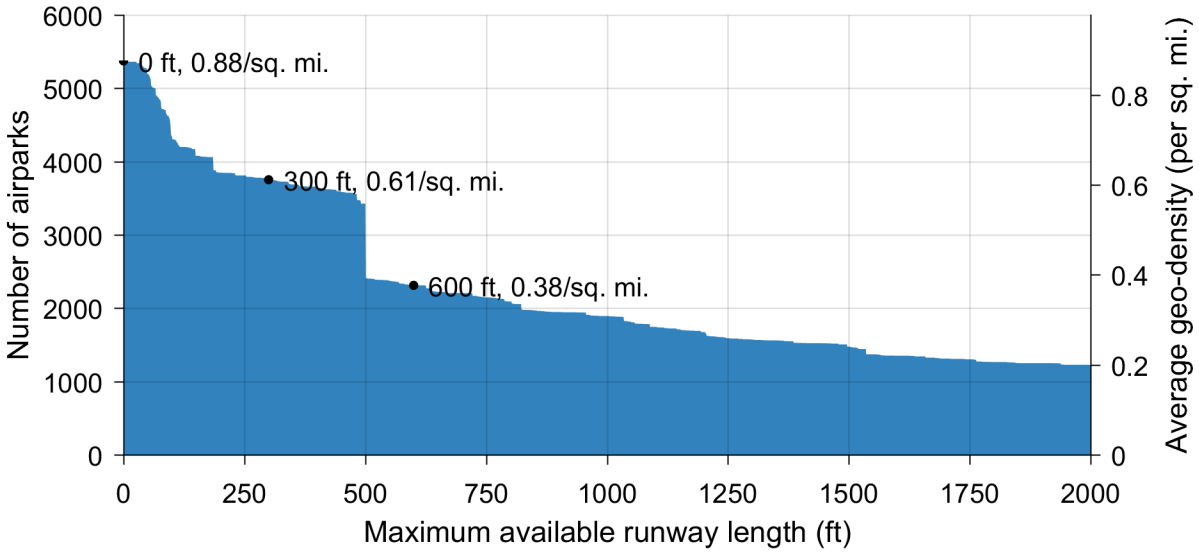

(a) Cumulative distribution function of barge construction type.

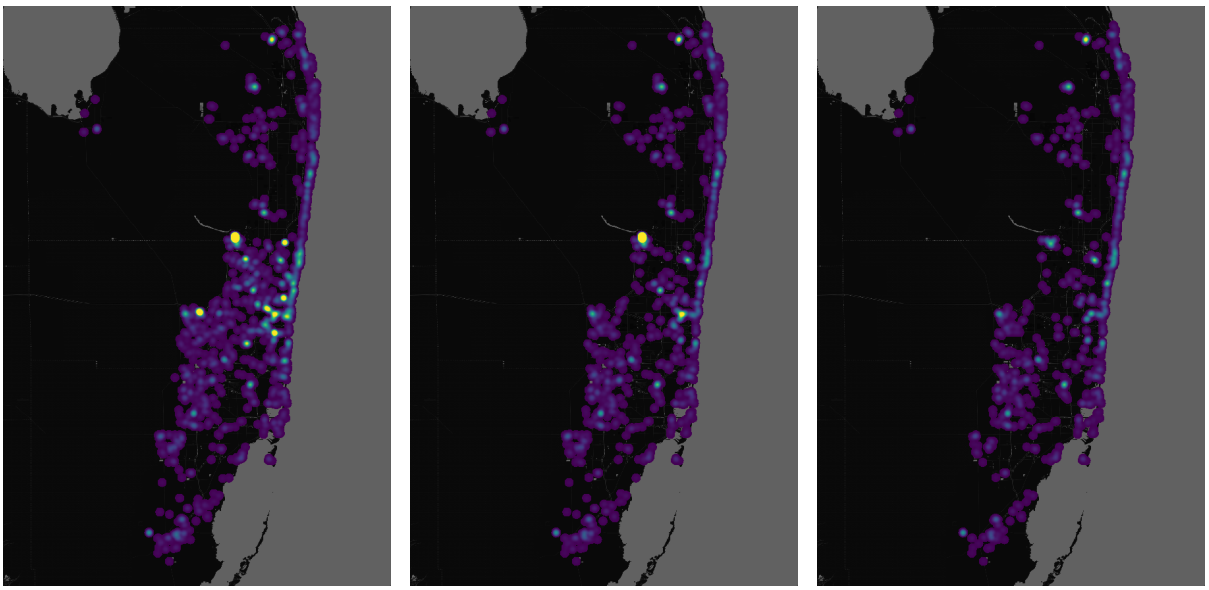

(b) Heatmap with no length limit. **(c) Heatmap at 300 ft length limit.** **(d) Heatmap at 600 ft length limit.**

Figure 13 Geo-density analysis of barge construction type.

Figure 13a plots the CDF of the barge construction type only. This construction type contains roughly half as many potential airpark locations as the vacant land construction type at its maximum, but is somewhat less sensitive to increases in runway field length. At 300 feet, there are still 69.3% of the maximum barge airpark locations remaining, compared to 62.6% for vacant land airparks. As runway length is further increased, this trend continues. At 600 feet, 43.2% of all barge airpark locations remain, compared to 28.4% of all vacant land airparks at the same runway length. Finally, the barge airpark distribution is much more favorable for extremely high runway lengths. At the extreme of

2000 feet, 1,225 barge airparks remain, or 22.8% of the maximum value. At the same runway length, only 172 vacant land airparks remain, or 1.8% of the maximum. Barge airparks can typically be built longer than vacant land airparks due to the large surface areas of the lakes, waterways, and oceans they occupy, and could potentially serve as a method to recover airpark geo-density if extremely high-performance STOL vehicles are technically infeasible or economically inviable.

Note the sharp drop-off in available barge airparks around 500 feet maximum available runway length. This drop-off is caused primarily by several undeveloped residential regions in Broward county. In this area, many homes are built around residential boat basins, which allow homeowners easy access to personal watercraft. Residential boat basins in developed areas are marked as unusable water bodies in this methodology, as they are not considered appropriate locations to build a large barge. However, boat basins built for residential use are not tagged as unusable water bodies by the county until they are incorporated into an active neighborhood. Thus, our geo-density methodology identifies a large number of potential barge airpark locations in the vacant lots that border these as-yet-unused boat basins, which are of a similar size as these communities are built using a common template. These high local relative geo-density regions can be seen as bright spots in the center of Fig. 13c that are not visible in Fig. 13d.

We can also see a bright line along the coast representing high local relative geo-density in Fig.s 13b, 13c, and 13d. This feature reflects barge airparks lining the Intracoastal Waterway and the coast of the Atlantic Ocean. These locations are typically very densely built, and the presence of these airparks reinforces the hypothesis that barge airparks would allow system designers to serve a much greater number of customers.

The CDF for the additive construction type is presented in Fig. 14a. This construction type presents far fewer opportunities for development than the vacant land or barge construction types, having a maximum available geo-density of only 0.12 airparks per square mile, which decreases to just 0.01 airparks per square mile at 600 feet. Thus, this construction type is recommended only to augment a larger system.

In particular, this construction type is well-suited to enable access to medium density communities that may have little vacant land space remaining, but do have a large amount of land occupied by surface parking lots. This effect can be seen in Fig. 14b, which shows the highest relative local geo-density in Broward County, which is in between Miami-Dade and Palm Beach Counties in population density and available vacant land.

Note the sharp drop-off in airpark geo-density between 500 and 600 feet maximum available runway length. Although the exact cause of this drop-off could not be determined, it may be due to inherent similarities in sizing between malls and big-box stores, which are typically built to follow one of several common templates to save on architecture and planning costs.

A CDF of all four airpark construction types, including pre-existing airparks, which were not shown independently due to the small size of that set, is presented in Fig. 15a. The overall system exhibits exceptionally high geo-density, with a maximum average airpark geo-density of 2.55 airparks per square mile. Although this geo-density drops sharply as takeoff field length increases, the previously-discussed characteristics of the barge airpark distribution limit this drop-off somewhat. At a maximum available runway length of 600 feet, the average geo-density is still 0.83 airparks per square mile, or 32.5% of the maximum available airpark geo-density. Additionally, the geo-density bottoms out at 23.0% of the maximum at 2000 feet thanks to the influence of the barge airpark construction type.

In Fig.s 15b, 15c, and 15d, we can see that this combination does a much better job of covering nearly all potential customers than any of the airpark construction types could independently. Figure 15c shows a significant level of geo-density for regions in Palm Beach County, the western and southern portion of Miami-Dade County, and the eastern coast of all three counties. The interior of the Miami metropolitan area, especially in Miami-Dade and Broward Counties, is not covered quite as well by the STOL ODM system due to the decreased amount of vacant land or suitable water bodies in this region.

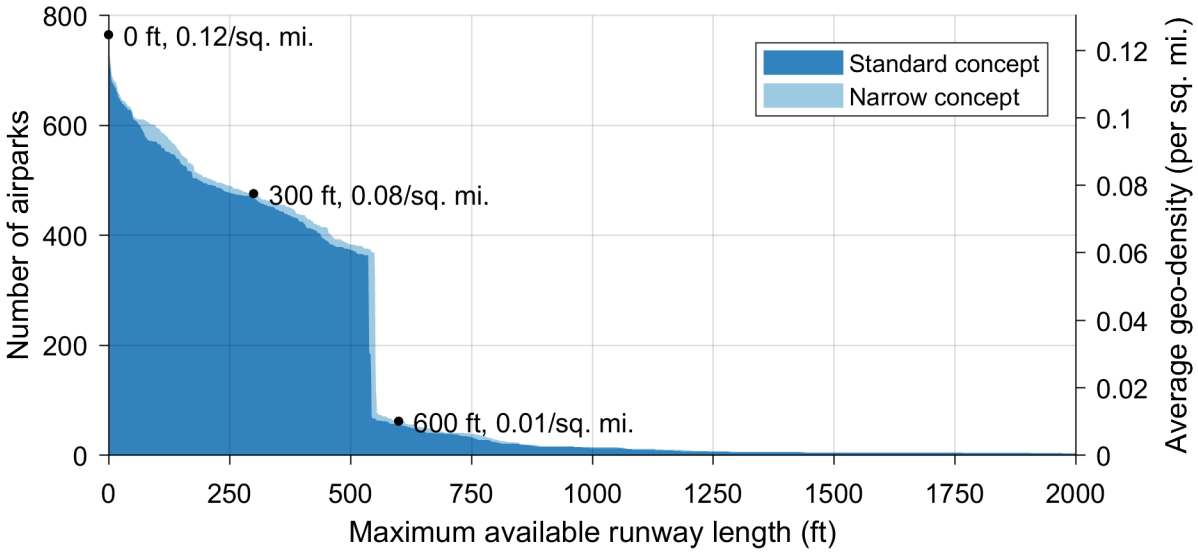

(a) Cumulative distribution function of additive construction type.

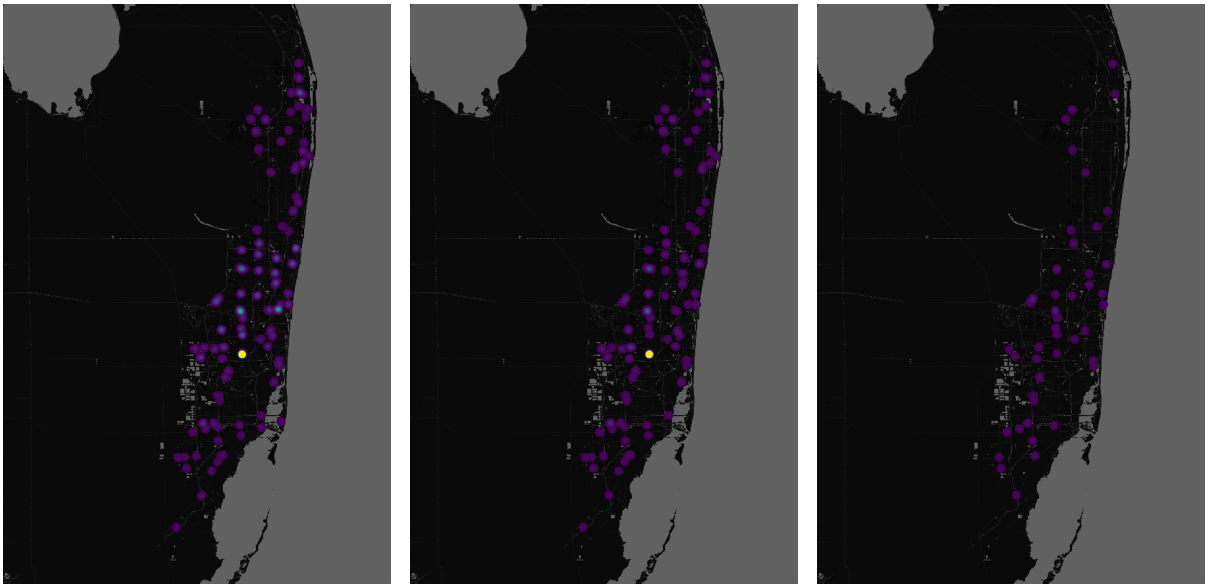

(b) Heatmap with no length limit. **(c) Heatmap at 300 ft length limit.** **(d) Heatmap at 600 ft length limit.**

Figure 14 Geo-density analysis of additive construction type.

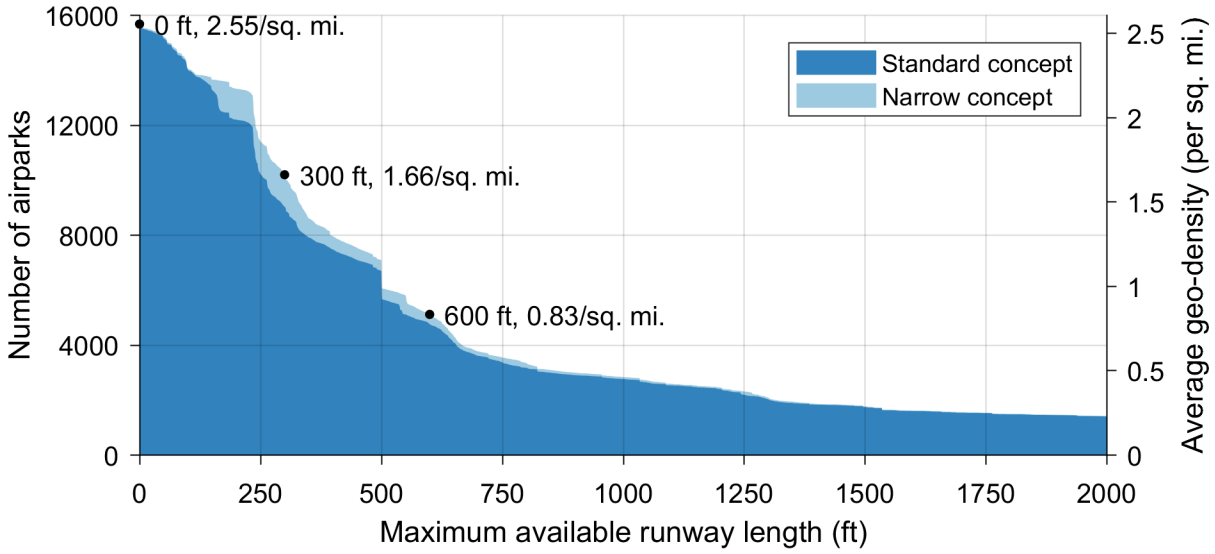

(a) Cumulative distribution function of all construction types.

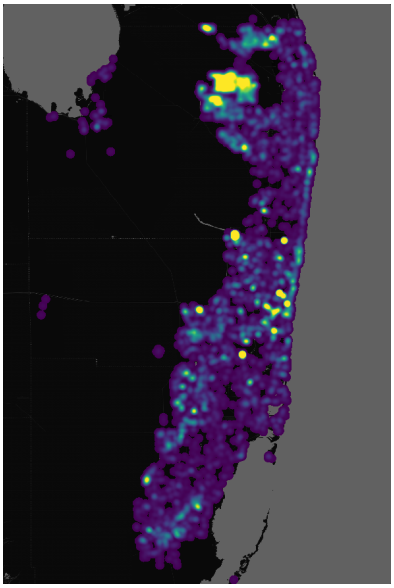

(b) Heatmap with no length limit.

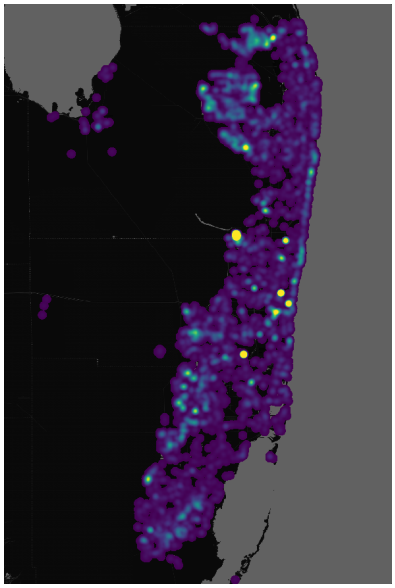

(c) Heatmap at 300 ft length limit.

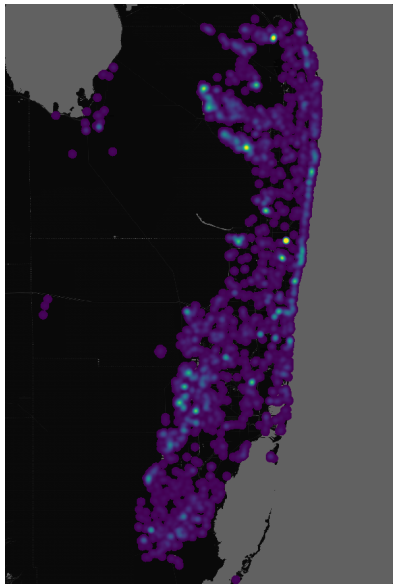

(d) Heatmap at 600 ft length limit.

Figure 15 Geo-density analysis of all construction types.

B. Sensitivity to Runway Safety Area

In Sec. IIB we introduced a runway safety area parameter, R, to replace the FAA recommended public safety area length on either end of the runway. As regulations for a potential STOL ODM system are purely hypothetical at this stage, parameterization of the safety area parameter is important to allow this methodology to adapt to future developments in this field. Additionally, the parameterization of the runway safety area length allows us to examine the impact of several regulatory scenarios on system feasibility.

The most likely regulatory constraint on this system would be a minimum overfly altitude over adjacent parcels. FAA regulations do not impose a specific altitude for takeoff or landing operations (14 CFR 91.119). However, this regulation is based on an aerial paradigm in which airports are typically placed far away from residential or other densely populated areas. As the goal of ODM aerial systems is to place airparks in densely populated regions, takeoff and landing overfly constraints may be imposed in the interest of public safety and wellbeing.

To model potential overfly requirements, we assume that the vehicle will have reached 35 feet in altitude at the point it passes the runway threshold, as this a common assumption in the calculation of takeoff field length requirements. The necessary runway safety area can then be found by calculating

$$R = \frac{h_{OF} - 35}{tan(\gamma)} \tag{3}$$

where h_{OF} is the prescribed overfly height, and γ is the departure flight path angle, which we will assume to be 15°, as in Sec. IID. Thus, the adjusted runway length for any parcel is given by

$$L_{adj} = L_{max} - 2 \times R \approx L_{max} - 2 \times 3.732(h_{OF} - 35) \tag{4}$$

where L_{max} is the calculated maximum runway length assuming no runway safety area.

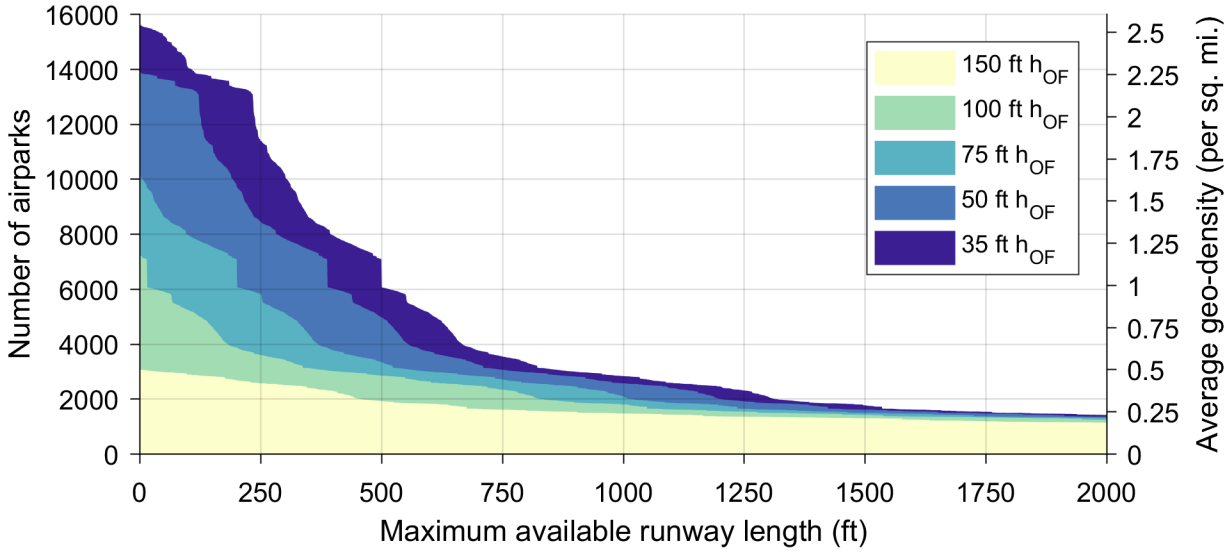

Figure 16 Sensitivity of geo-density to overfly requirement.

Figure 16 presents a modified CDF for all airpark construction types with varying overfly altitude requirements imposed using the previously described methodology. As we can see, overfly requirements drastically affect the overall airpark geo-density, and thus system feasibility as a whole. Requiring a 75 foot altitude before crossing over to the adjacent parcel reduces maximum average geo-density from 1.66 airparks per square mile to 0.84 airparks per square mile, assuming a 300 foot long runway with no overfly requirement. As we approach higher minimum overfly requirements, the available geo-density drops even further, especially as we impose stricter minimum runway length requirements.

C. Comparison to Other Transportation Networks

We can determine a first-pass assessment of STOL ODM system feasibility by comparing STOL ODM geo-density to the geo-density of other preexisting or proposed transportation networks.

In a NASA study on ODM VTOL operations [6], the authors found a total of 200 potential helipad cites over 280 square miles in the Silicon Valley area, resulting in an average geo-density of 0.71 vertiports per square mile. In a separate portion of the paper, the authors identified 50 potential coastal heliports covering 47 square miles in San Francisco, resulting in an average geo-density of 1.06 vertiports per square mile. Our STOL ODM airpark placement methodology achieves an average geo-density of 1.06 airparks per square mile with a runway length of 500 feet using all airpark construction types, or a runway length of 271 feet using only the vacant land construction type, assuming no overfly requirement is imposed.

It is also pertinent to compare the hypothetical STOL ODM system to preexisting conventional public transportation methods. The New York City Subway, widely considered to be the most successful public transportation system in the US. This system serves a total land area of 244.83 square miles using 472 stations, resulting in an average geo-density of 1.92 stations per square mile. This level of geo-density is achieved by the STOL ODM system at a runway length of 244 feet using all available construction types and assuming no overfly restrictions.

The London Underground serves a total area of 606 square miles using 270 stations, resulting in an average geo-density of 0.45 stations per square mile. This level of geo-density is achieved by the STOL ODM system at a runway length of 1,033 feet using all available airpark types, or 596 feet using only vacant land airparks, assuming no overfly restrictions.

D. Expansion to Other Counties

In order to validate the methodology presented in this paper, we repeated the process on Lee and Collier Counties, two nearby counties situated west of Miami encompassing 3,517 square miles and approximately one million residents. Applying the process to these counties also enables future analysis of the STOL ODM system over longer routes than are available in the Miami metropolitan area alone.

We repeated the previously described geo-density methodology for the vacant land construction type only. These results are presented in Fig. 17. Note that Lee and Collier Counties have a much lower overall geo-density than the Miami metropolitan region. The maximum available geo-density in Lee and Collier counties is 0.48 airparks per square mile, compared to 0.97 airparks per square mile for the Miami metropolitan area using only the vacant land construction type, assuming a 300 foot runway with no overfly requirements. This is likely due to Lee and Collier counties having a larger amount of land that is unsuitable for airpark construction due to its status as protected or agricultural land, which have not been selected as airpark locations in this study.

However, the sensitivity of airpark geo-density to maximum available runway length is less extreme in Lee and Collier Counties than in the Miami metropolitan area. This is most likely due to parcels in these counties being larger on average than parcels in the Miami metro due to the lower overall population density of the region.

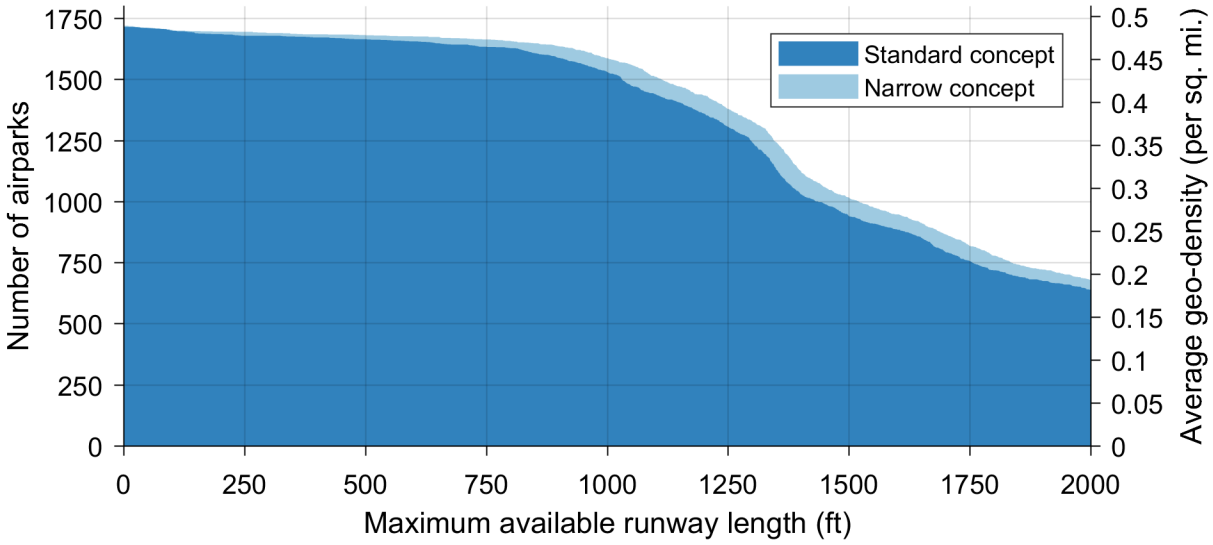

(a) Cumulative distribution function of vacant land construction type in Lee and Collier Counties.

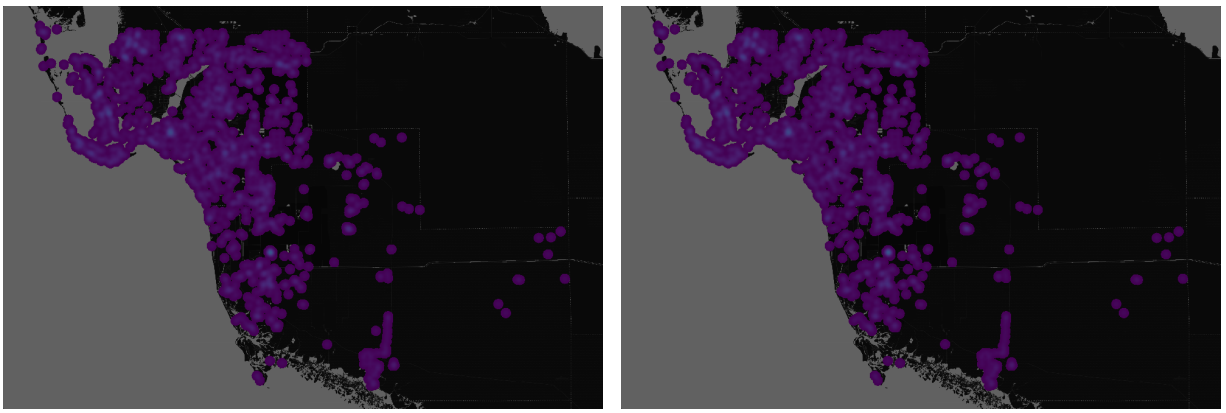

(b) Heatmap with no length limit.

(c) Heatmap at 600 ft length limit.

Figure 17 Geo-density analysis of vacant land construction type in Lee and Collier Counties.

IV. Conclusions

The methodology presented in this paper allows system designers to rapidly place a large number of airparks in a metropolitan region of interest and assess the sensitivity of the resultant airpark geo-density to a number of different factors. Although this methodology can only approximate an actual airpark site selection process, it provides a first-pass estimate of the end results of such a process, which is critical for enabling future studies concerning the technological feasibility, operational feasibility, and economic viability of a STOL ODM transportation system.

Analysis of individual airpark construction types, including vacant land construction, barge construction, additive construction, and preexisting airport incorporation, shows the importance of creating unique and innovative airpark concept designs to both increase average airpark geo-density and serve customers in the most dense portions of the region. However, airpark geo-density shows extreme sensitivity to vehicle takeoff performance and potential takeoff overfly constraints. Thus, high performance STOL vehicle designs and practical regulations are critical to enabling the success of STOL ODM systems.

Future work will expand on this research by both improving the fidelity of this analysis and using the results in overall system performance analyses. The airpark fitting algorithm used in this paper will be updated to incorporate wind effects by imposing a penalty function related to the local wind magnitude and direction on the maximum calculated runway length for each heading. The results produced by this paper will be used in future studies related to system

performance characteristics such as the travel time of commuters using the STOL ODM system [22]. These results will also be used to drive balanced field length requirements for STOL vehicle designs, allowing a detailed economic assessment of the system to be performed.

Acknowledgments

The authors would like to thank Dr. Michael Patterson and Mr. Kenneth Goodrich of NASA Langley Research Center for their support and advice over the course of this research. We would also like to thank Mr. Rich Ouellette of Boeing for advising us in the area of STOL concept vehicle design. We would also like to thank Georgia Tech students Lansing Wei, Brandon Leung, Lourenço Jara de Carvalho, Alaric Gregoire, Eddie Li, and Philip Patterson for their contributions to this research.

References

[1] "Fast-Forwarding to a Future of On-Demand Urban Air Transportation," Web, Oct. 2016. Uber Elevate.

[2] Justin, C. Y., Payan, A. P., Briceno, S. I., and Mavris, D. N., "Operational and Economic Feasibility of Electric Thin Haul Transportation," *17th AIAA Aviation Technology, Integration, and Operations Conference*, American Institute of Aeronautics and Astronautics, 2017. doi:10.2514/6.2017-3283.

[3] Harish, A., Perron, C., Bavaro, D., Ahuja, J., Ozcan, M., Justin, C. Y., Briceno, S. I., German, B. J., and Mavris, D., "Economics of Advanced Thin-Haul Concepts and Operations," *16th AIAA Aviation Technology, Integration, and Operations Conference*, American Institute of Aeronautics and Astronautics, 2016. doi:10.2514/6.2016-3767.

[4] German, B., and McDonald, R., "eVTOL Stored Energy Overview," , Apr. 2017. Uber Elevate Summit.

[5] Stoll, A. M., Stilson, E. V., Bevirt, J., and Pei, P. P., "Conceptual Design of the Joby S2 Electric VTOL PAV," , Jun. 2014. Aviation Technology, Integration, and Operations Conference.

[6] Antcliff, K. R., Moore, M. D., and Goodrich, K. H., "Silicon Valley as an Early Adopter for On-Demand Civil VTOL Operations," , Mar. 2016. On-Demand Mobility/Emerging Tech Workshop.

[7] Stoll, A. M., Bevirt, J., Moore, M. D., Fredericks, W. J., and Borer, N. K., "Drag Reduction Through Distributed Electric Propulsion," *14th AIAA Aviation Technology, Integration, and Operations Conference*, American Institute of Aeronautics and Astronautics, 2014. doi:10.2514/6.2014-2851.

[8] "P750 XSTOL Technical Specifications," Pacific Aerospace, n.d.. URL http://www.aerospace.co.nz/aircraft/p-750-xstol/specifications, accessed 2018-05-15.

[9] "Su-80 Specifications," Sukhoi Company, n.d.. URL http://sukhoi.org/eng/planes/civil/su-80/characteristic/, accessed 2018-5-15.

[10] "Hornet STOL Performance Data," Australian Aircraft Kits, n.d.. URL http://www.aircraftkits.com.au/documents/Hornet_STOL_Performance_Data_March1012.pdf, accessed 2018-5-15.

[11] "Kodiak," Quest Aircraft, n.d.. URL http://questaircraft.com/kodiak/, accessed 2018-5-15.

[12] "Performance of the State-of-the-Art US-2," ShinMaywa Industries, n.d.. URL http://www.shinmaywa.co.jp/aircraft/english/us2/us2_capability.html, accessed 2018-5-15.

[13] "STOL CH 801: Four-seat short take-off and landing sport utility kit aircraft," Zenith Aircraft Company, n.d.. URL http://www.zenithair.com/stolch801/index1.html, accessed 2018-5-15.

[14] Maliene, V., Wignall, L., and Malys, N., "Brownfield Regeneration: Waterfront Site Developments in Liverpool and Cologne," *Journal of Environmental Engineering and Landscape Management*, Vol. 20, No. 1, 2012, pp. 5–16. doi: 10.3846/16486897.2012.659030.

[15] "A Map of Florida's Counties," US Census Bureau, n.d. URL http://quickfacts.census.gov/qfd/maps/florida_map.html, accessed 2018-5-15.

[16] Seeley, B. A., "Regional Sky Transit IV: Pocket Airpark Design Constraints," *17th AIAA Aviation Technology, Integration, and Operations Conference*, American Institute of Aeronautics and Astronautics, 2017. doi:10.2514/6.2017-3440.

[17] "Property Tax - Data Portal - Request Assessment Roll and GIS Data," Florida Department of Revenue, 2018. URL http://floridarevenue.com/property/Pages/DataPortal_RequestAssessmentRollGISData.aspx, accessed 2018-5-15.

[18] Wakefield, I., and Dubuque, C., "Exceeding Tire Speed Rating During Takeoff," Boeing AERO Quarterly, Jun. 2009.

[19] Knauer, C., Schlipf, L., Schmidt, J. M., and Tiwary, H. R., "Largest inscribed rectangles in convex polygons," *Journal of Discrete Algorithms*, Vol. 13, 2012, pp. 78–85. doi:10.1016/j.jda.2012.01.002.

[20] Molano, R., Rodríguez, P. G., Caro, A., and Durán, M. L., "Finding the largest area rectangle of arbitrary orientation in a closed contour," *Applied Mathematics and Computation*, Vol. 218, No. 19, 2012, pp. 9866 – 9874. doi:https://doi.org/10.1016/j.amc.2012.03.063.

[21] Smilkov, D., "Largest rectangle in a polygon," Web, Jul 2014.

[22] Wei, L., Justin, C. Y., Briceno, S. I., and Mavris, D. N., "Door-to-Door Travel Time Comparative Assessment for Conventional Transportation Methods and Short Takeoff and Landing On Demand Mobility Concepts," , Jul. 2018. Submitted for publication.